Miniband formation in a quantum dot crystal

Olga L. Lazarenkova[a] and Alexander A. Balandin[b]
Department of Electrical Engineering, University of California at Riverside, Riverside, California 92521

(Received 25 January 2001; accepted for publication 23 February 2001)

We analyze the carrier energy band structure in a three-dimensional *regimented* array of semiconductor quantum dots using an envelope function approximation. The coupling among quantum dots leads to a splitting of the quantized carrier energy levels of single dots and formation of three-dimensional minibands. By changing the size of quantum dots, interdot distances, barrier height, and regimentation, one can control the electronic band structure of this artificial *quantum dot crystal*. Results of simulations carried out for simple cubic and tetragonal quantum dot crystal show that the carrier density of states, effective mass tensor and other properties are different from those of bulk and quantum well superlattices. It has also been established that the properties of artificial crystal are more sensitive to the dot regimentation rather then to the dot shape. The proposed engineering of three-dimensional mini bands in quantum dot crystals allows one to fine-tune electronic and optical properties of such nanostructures. © *2001 American Institute of Physics.*
[DOI: 10.1063/1.1366662]

I. INTRODUCTION

Quantum dots represent the ultimate case of spatial confinement for electrons and holes. This creates an exciting opportunity for controlled modification of carrier states in these entities, and re-engineering of optical, electronic, and thermoelectric properties of many technologically important semiconductor materials.[1–3] In most cases, it is more practical to deal with arrays of semiconductor quantum dots or multiple arrays, e.g., stacks of quantum dots, which are also referred to as quantum dot superlattices (QDS).[3,4] Quantum dot arrays grown by molecular beam epitaxy (MBE) can be completely random,[5,6] partially regimented, such as QDS with vertical dot site correlation,[3,4] or may have very high degree of regimentation.[7,8] The self-organization of pyramidal PbSe islands during strained-layer epitaxial growth of $PbSe/Pb_{1-x}Eu_xTe$ has resulted in the formation of three-dimensional (3D) quantum dot crystals with the dots arranged in a trigonal lattice with a face-centered-cubic-like vertical stacking sequence.[7] Recently, the tuning of lateral and vertical regimentation in self-organized QDS by changes in the spacer thickness and growth conditions has been demonstrated.[8] Other quantum dot synthesis techniques, such as electrochemical self-assembly, have also led to a high degree of lateral regimentation resulting in hexagonal quantum dot arrays.[9,10]

In comparison to conventional quantum well superlattices[11] or multiple quantum well structures,[12] QDS that consists of multiple arrays of quantum dots may have many advantages in applications due to its modified density of electronic states and optical selection rules. For example, due to relaxed intraband optical selection rules in QDS, they are capable of absorbing normally incident radiation[3,4] while it is not possible in quantum well superlattices. The latter makes QDS a good candidate for infrared photodetector applications. QDS based on Si/Ge material system has also been recently proposed for applications as a high-temperature thermoelectric element.[13] Many more applications are envisioned for *regimented* QDS.[2] Although different types of regimented QDS had already been fabricated using self-assembly techniques,[7–10] very little attention has been paid to theoretical description of carrier and phonon transport in such structures.[13,14]

In this article, we analyze the carrier energy band structure in a 3D *regimented* array of semiconductor quantum dots using an envelope function approximation. The regimentation, e.g., spatial site correlation, along all three directions results in the formation of an artificial crystal, where quantum dots play the role of atoms. Thus, we refer to this structure as a *quantum dot crystal* (QDC). We particularly focus our attention on orthorhombic and simple cubic QDC that consist of very small (feature size on the order of 5–10 nm) Ge quantum dots grown on Si and surrounded by Si cap layer. In the next section, we outline the theoretical formalism used for calculating 3D energy minibands and the effective mass tensor. It is followed by Sec. III, which presents results of the numerical simulation and discussion. Our conclusions are given in Sec. IV.

II. FORMALISM

For simplicity, we restrict our analysis to orthorhombic symmetry for both the QDS and the single quantum dot as shown in Fig. 1(a). Thus, the electron dispersion relation derived here is valid for QDCs of $Fddd(D_{2h}^{24})$ and some higher space symmetry groups. Here, we consider simple cubic and tetragonal structures as particular cases of *orthorhombic* lattice symmetry. These structures are similar to MBE grown Ge/Si QDS with vertical site correlation.[3,4] We

[a]On leave from the Microelectronics Department, St. Petersburg State Electrotechnical University ''LETI,'' St. Petersburg, Russia; electronic mail: omk.me@eltech.ru
[b]Author to whom correspondence should be addressed; electronic mail: alexb@ee.ucr.edu

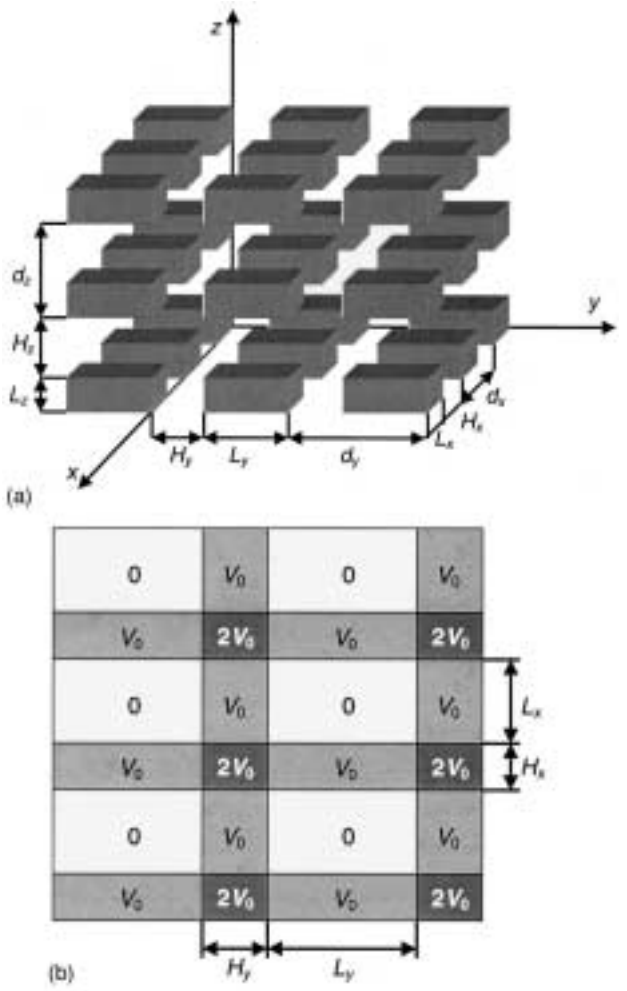

FIG. 1. (a) Schematic structure of the orthorhombic QDC; and (b) confining potential for the region $|z-n_z d_z| \leq L_z/2$. Note that the carrier states in quantum dots are mostly determined by interaction with nearest-neighboring dots separated from each other by the potential V_0.

neglect phenomena associated with the ''true'' Bloch functions of carriers that have the periodicity of an atomic scale. Instead, we focus our attention on the envelope functions that enter our formalism as *quasi* Bloch functions for the QDC. In Fig. 1(a) we also show the notations used throughout the rest of the article.

Theoretical models for quantum dots within the envelope function approximation usually lead to a complex multidimensional Schrodinger equation, which needs to be solved using finite elements method,[15] or plane wave expansion.[14] Application of the pseudopotential methods for QDC is computationally challenging. The goal of this work is to develop a simple, almost analytical, formalism for carrier transport in QDC that would serve as a useful tool for experimentalists and materials growers. Thus, we chose a specific form of the confining potential that allows us to simplify the problem in real space yet giving a rather accurate description of the carrier transport in realistic structures.

Let us consider the motion of a charge carrier in a host crystal in the presence of the additional potential $V(\mathbf{r})$. We assume the structure to be isomorphic with defect-free interfaces. We restrict our analysis to heavy holes in Ge/Si QDC. This is done for several reasons. First of all, there is a significant practical interest to this material system. Second, most of the band gap discontinuity between Si and Ge goes to the valence band. Third, the potential energy maximum in the valence band is located in Γ point, which greatly simplifies the model and justifies our omission of carrier Bloch functions from consideration.

The Schrödinger equation that describes the motion of a single hole in such a system can be written in the following form

$$\left[-\frac{\hbar^2}{2}\nabla_r \frac{1}{m^*(\mathbf{r})}\nabla_r + V(\mathbf{r})\right]\varphi(\mathbf{r}) = E\varphi(\mathbf{r}). \tag{1}$$

Here, the atomic structure of the host semiconductor enters the analysis as an effective mass m^*. This parameter assumes different values in the quantum dot and the barriers. The potential $V(\mathbf{r})$ corresponds to an infinite sequence of quantum dots of size L_x, L_y, and L_z separated by the barriers of thickness H_x, H_y, and H_z. We assume that it is written as a sum of three independent periodic functions of coordinates x, y, and z with periods of d_x, d_y, and $d_z(d_\xi = L_\xi + H_\xi)$:

$$V(\mathbf{r}) = V_x(x) + V_y(y) + V_z(z), \tag{2}$$

where

$$V_\xi(\xi) = \begin{cases} 0 & \text{if } |\xi - \eta_\xi d_\xi| \leq L_\xi/2 \\ V_0 & \text{if } |\xi - \eta_\xi d_\xi| > L_\xi/2 \end{cases}. \tag{3}$$

Here η_ξ are the integer numbers and subscript ξ denotes a particular coordinate axis. This choice of potential allows us to separate the carrier motion along three coordinate axes. The 3D Schrödinger equation decouples in this case into three identical one-dimensional (1D) quantum-well superlattice equations. The 3D envelope wave function $\varphi(\mathbf{r})$ can therefore be presented as a product of three 1D eigenfunctions χ_ξ in the following way

$$\varphi(r) \equiv \varphi_{n_x,n_y,n_z}(x,y,z) = \chi_{n_x}(x)\chi_{n_y}(y)\chi_{n_z}(z). \tag{4}$$

Here n_ξ denote the quantum number. The total energy spectrum for this wave function is given by

$$E_{n_x n_y n_z} = E_{n_x} + E_{n_y} + E_{n_z}, \tag{5}$$

where E_n are the eigenvalues of the one-dimensional Schrödinger's equation.

For the chosen geometry of QDC and band offsets the carrier wave functions and energy spectrum are *mostly* determined by the nearest-neighbor interaction between dots separated by the potential barrier V_0. The corner potentials induce only minor corrections, which are particularly small for the below-the-barrier states. This observation is important because the confining potential of Eqs. (2) and (3) does not describe a simple QDC of a rectangular quantum dot surrounded by the potential barrier of the *equal* height. In two dimensions, this situation is illustrated in Fig. 1(b). The dots are separated from their nearest neighbors by a potential barrier of the height V_0, but in the corners, the height of the potential barrier is $2V_0$. Similarly, in 3D, there exist outer regions where the overlap of 1D potentials along each axes

gives rise to a potential barrier of $3V_0$. Thus, our *exact* solution for a given potential of Eqs. (2) and (3) presents a very good approximation for more realistic QDC potentials with the constant barrier height.

The solution of Eq. (1) with the potential of Eqs. (1) and (2) has the form familiar from the Kronig–Penny model[16]

$$\cos(q_\xi d_\xi)=\cos(k_\xi^W L_\xi)\cos(k_\xi^B H_\xi)-\frac{1}{2}\left(\frac{k_\xi^B m_W^*}{k_\xi^W m_B^*}+\frac{k_\xi^W m_B^*}{k_\xi^B m_W^*}\right)\times\sin(k_\xi^W L_\xi)\sin(k_\xi^B H_\xi)\quad \text{if } E_\xi \geqslant V_0, \tag{6a}$$

$$\cos(q_\xi d_\xi)=\cos(k_\xi^W L_\xi)\cosh(k_\xi^B H_\xi)-\frac{1}{2}\left(-\frac{k_\xi^B m_W^*}{k_\xi^W m_B^*}+\frac{k_\xi^W m_B^*}{k_\xi^B m_W^*}\right)\sin(k_\xi^W L_\xi)\sinh(k_\xi^B H_\xi)\quad \text{if } 0<E_\xi<V_0, \tag{6b}$$

where

$$k_\xi^B=\frac{\sqrt{2m_B^*|E_\xi-V_0|}}{\hbar},\quad k_\xi^W=\frac{\sqrt{2m_W^*|E_\xi|}}{\hbar}. \tag{7}$$

The effective masses m_B^* and m_W^* used in Eqs. (6) and (7) depend on the crystallographic orientation of the quantum dot interfaces. Equations (6) and (7) allow us to calculate the carrier dispersion relation $E(\mathbf{q})=E_x(q_x)+E_y(q_y)+E_z(q_z)$ in the QDC. Since for each given value of q_ξ there is an infinite number of solutions, we use the miniband index n_ξ to label the carrier energy.

In the next section, we show that despite the simplicity of the theoretical formalism used, it is capable of capturing new features characteristic for 3D artificial QDC that are not present in real bulk crystals and quantum well superlattices.

III. RESULTS AND DISCUSSION

We carry out our analysis of the 3D minibands in the *artificial* QDC, on the example of Si/Ge material system. The considered structure is similar to the multiple arrays of small Ge quantum dots grown on (001) Si by solid-source MBE.[3,4] Approximately 90% of the band offset in such a structure goes to the valence band.[4] The interaction between heavy and light-hole states is neglected because they are significantly split by the strain,[16] and the light-hole states are above the barrier. The band offset for the heavy holes is approximately equal to 0.45 eV.[17] In our calculations, we used the following values for the effective masses $m_W^*=m_{\mathrm{Ge}}^*=0.28\,m_0$ and $m_B^*=m_{\mathrm{Si}}^*=0.49\,m_0$. Microscopy has shown that most of self-organized quantum dots have a pyramidal or *hut cluster* form with dimensions of 10–100 nm.[1] Thus, a single dot could be thought of as a finite-barrier cubic dot with four additional perturbing potentials.[18] The latter justifies our assumption of orthorhombic QDC. Moreover, as it will be shown, the band structure is much more sensitive to the dot regimentation rather than to the dot shape.

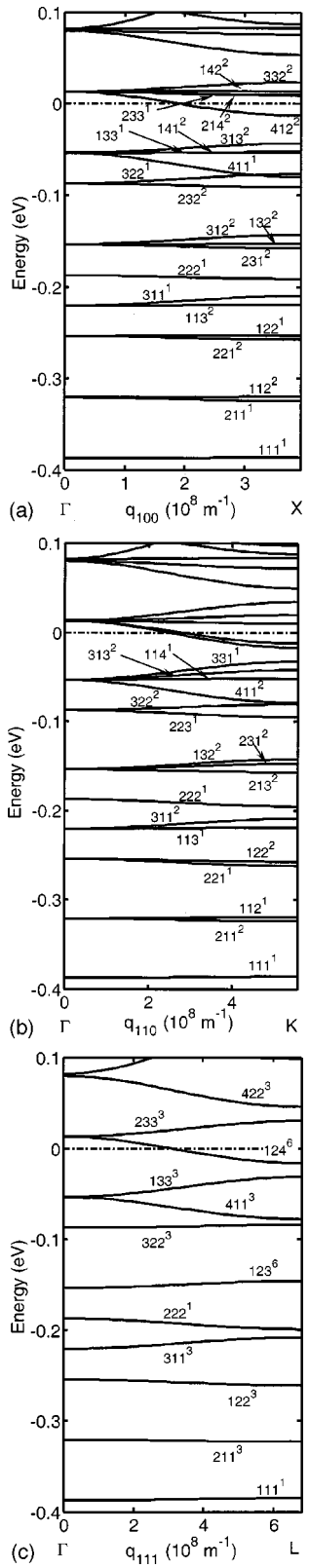

FIG. 2. Dispersion relation in a cubical QDC shown along [[100]], [[110]], and [[111]] quasi crystallographic directions in (a), (b), and (c), respectively. The energy in units of eV is counted from the position of the potential barrier. The dot size is $L_x=L_y=L_z=6.5$ nm and the interdot distance is $H_x=H_y=H_z=1.5$ nm. Material parameters used in simulation correspond to the valence band of Ge/Si system.

Figures 2(a)–2(c) present hole dispersion in a *simple cubic* QDC along three *quasi* crystallographic directions. For convenience, the energy is counted from the position of the potential barrier. One should emphasis here that directions denoted as [[100]], [[110]], and [[111]] are associated with the ordering of the quantum dots and are not related to the three high-symmetry directions of the Si crystal itself. In order to distinguish quasicrystallographic directions, we use double square brackets in the rest of this article. The carrier wave vector is denoted by **q** with subscript showing particular quasi crystallographic direction. Zero energy along the ordinate axis corresponds to the position of the potential barrier. The results in Fig. 2 are shown for a QDC that consists of quantum dots with the size $L=6.5$ nm and interdot distance $H=1.5$ nm. The energy bands are denoted by three quantum numbers $n_x n_y n_z$ with the superscript indicating the degeneracy of the band. Note that here the spin degeneracy is not counted. It will be taken into account below when we calculate the carrier density of states. Like in real crystals, the energy in QDC has the full symmetry of the reciprocal lattice. It repeats both translation and point group symmetry of the crystal, in addition to the time reversal symmetry resulting in $E(\mathbf{q})=E(-\mathbf{q})$. The energy bands shown in Fig. 2 are degenerated in the center of the *quasi* Brillouin zone (QBZ) of the artificial crystal. The highest, sixfold, degeneracy is achieved in minibands of cubical QDC characterized by different quantum numbers $n_x n_y n_z$. If two of these three quantum numbers are equal, the degeneracy is threefold. Finally, if $n_x=n_y=n_z$ there is no symmetry degeneracy in such a miniband. Moving from the point of high symmetry in the center of the QBZ to a point of lower symmetry, the energy bands split.

Unlike in real crystals, where it is difficult to find degeneracy more than twofold away from the highly symmetrical points of the Brillouin zone,[19] in artificial cubical QDC the degeneracy can be up to sixfold along [[111]] quasi crystallographic direction even far from the center of QBZ. It is achieved when both the quantum dot sizes and the interdot distances are equal along all three axes [see Fig. 2(c)]. This degeneracy is a result of the same symmetry of the dot and the superlattice. If their symmetries are different, the twofold degeneracy will be the maximum permitted in all directions. One can see from Fig. 2 that an incidental degeneracy (or zone crossing) can happen in the center of the QBZ.[20] The latter results in a complicated energy dependence of the carrier density of states (DOS).

A carrier DOS, which is a number of carrier states in an interval of energy per unit volume, is an important for virtually all electronic and optical applications of semiconductor structures. From elementary considerations DOS, denoted as $G(E)$, is given by

$$G(E)=\frac{2}{dE}\int d^3\mathbf{q}. \tag{8}$$

The integral is to be taken over the volume of the **q** space bounded by a surface of constant energy E. The factor 2 reflects the two-fold electron spin degeneracy. The results of our numerical simulation of DOS in a cubical quantum dot crystal are presented in Figs. 3(a)–3(c) for 3D minibands with different symmetry. The parameters of QDC are chosen to be the same as those used in Fig. 2. The arrows in Fig. 3 indicate particular quasi crystallographic points. The points of high symmetry correspond to analytic critical points with van Hove singularities. Note that the shape of DOS is de-

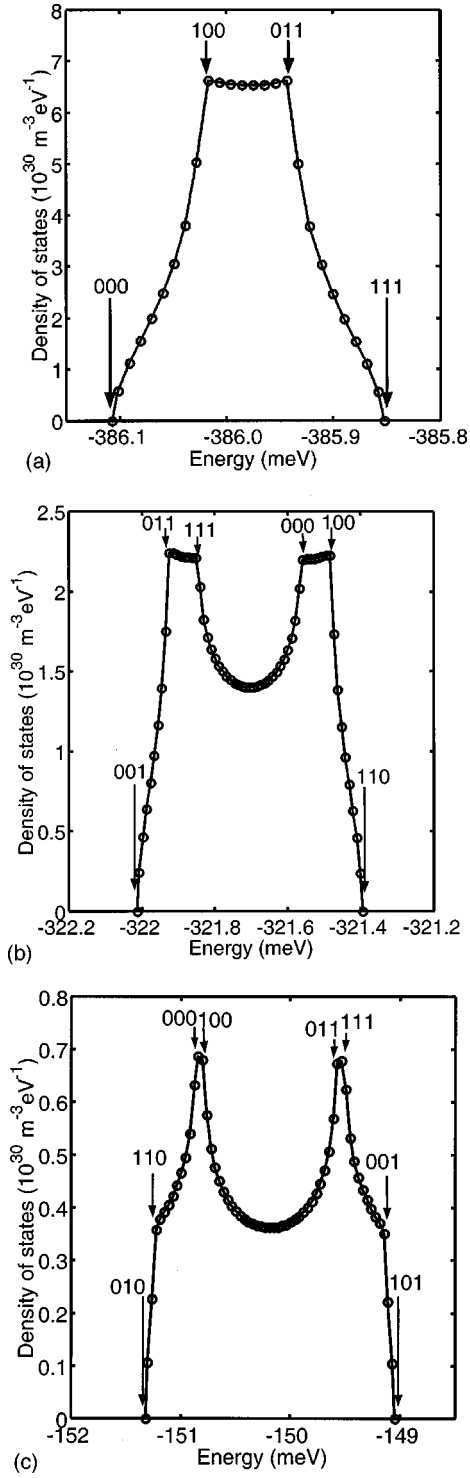

FIG. 3. DOS in a cubical QDC for 3D minibands defined by the following quantum numbers: (a) $n_x=n_y=n_z=1$; (b) $n_x=n_y=1$ and $n_z=2$; and (c) $n_x=1$, $n_y=2$, and $n_z=3$. The dot size is $L_x=L_y=L_z=6.5$ nm and the interdot distance is $H_x=H_y=H_z=1.5$ nm. The arrows indicate particular quasi crystallographic points. The energy in units of meV is counted from the position of the potential barrier. Note that the QDC DOS is different from that in bulk and in quantum well superlattices.

fined by the quantum numbers of the corresponding miniband. The one shown in Fig. 3(a) corresponds to quantum numbers $n_x=n_y=n_z$; while those shown in Figs. 3(b) and 3(c) correspond to $n_x>n_y=n_z$, $n_x=n_y<n_z$ or $n_x=n_z<n_y$; and $n_x\neq n_y\neq n_z$, respectively. In cubical QDC, the minibands that correspond to the cases shown in Figs. 3(b) and 3(c) can be symmetry degenerated up to three and six, respectively. Thus, in calculating DOS one has to multiply $G(E)$ by this degeneracy factor. One should mention here that the areas under each DOS curve, e.g., integral of each DOS, are all equal and defined by the density of quantum dots in a crystal.

Although the formalism that we used is rather simple it captures the specific features of electron transport in QDC. Thus, the obtained DOS is different from that in conventional quantum well superlattices with finite potential barrier. In quantum well superlattices, the electron DOS has an arccosine-like form superimposed over characteristic ''staircase'' due to two-dimensional 2D electron continuum in planes perpendicular to the growth direction.[21] The situation is obviously different in the quantum dot crystal [see Figs. 3(a)–(c)]. Although for the lowest miniband, the DOS in the artificial crystal has an arccosine-like edge, it drops down to zero at some higher energy since there is no 2D continuum [Fig. 3(a)], and becomes much more complicated for the next minibands [Figs. 3(b) and 3(c)].

The formation of 3D minibands in QDC is illustrated in Figs. 4(a)–4(b). It is well known that a single quantum dot has discrete spectrum below a potential barrier and continuous spectrum above the potential barrier. When quantum dots are separated by a finite barrier and positioned very close to each other so that there is a significant wave function overlap, the discrete energy levels split into minibands. This can be seen in Fig. 4(a) for the interdot distance H below 3 nm. Note that this value is calculated for Si/Ge system. For other material systems, such as InAs/GaAs, the splitting will occur at much larger distances. As the interdot distance increases, and the wave function overlap decreases, the minibands below the potential barrier reduce to discrete levels. This behavior is expected and consistent with what one observes in conventional quantum well superlattices. The 3D regimentation of quantum dots in QDC leads to appearance of ''resonant'' quasidiscrete energy levels above the potential barrier V_0 for large interdot distances ($H>4$ nm for Si/Ge) as seen in Fig. 4(a). These separate levels form due to the 3D periodicity of carrier envelopes, which appear in the equations describing the artificial crystal as quasi Bloch functions. It is interesting to note that the nature of these separate energy levels is entirely different from that of discrete states below the barrier. The former are the states defined by infinitely extended wave functions arising due to Born–von Karman periodic boundary conditions while the latter are essentially localized states. Figure 4(b) demonstrates a transformation of QDC minibands into discrete levels below the potential barrier and quasicontinuum above the barrier. Other important observations to make in Fig. 4(b) are that the miniband width does not increase monotonously with the energy, and that for realistic interdot distances complete energy gaps (stop bands) are formed in QDC. In real

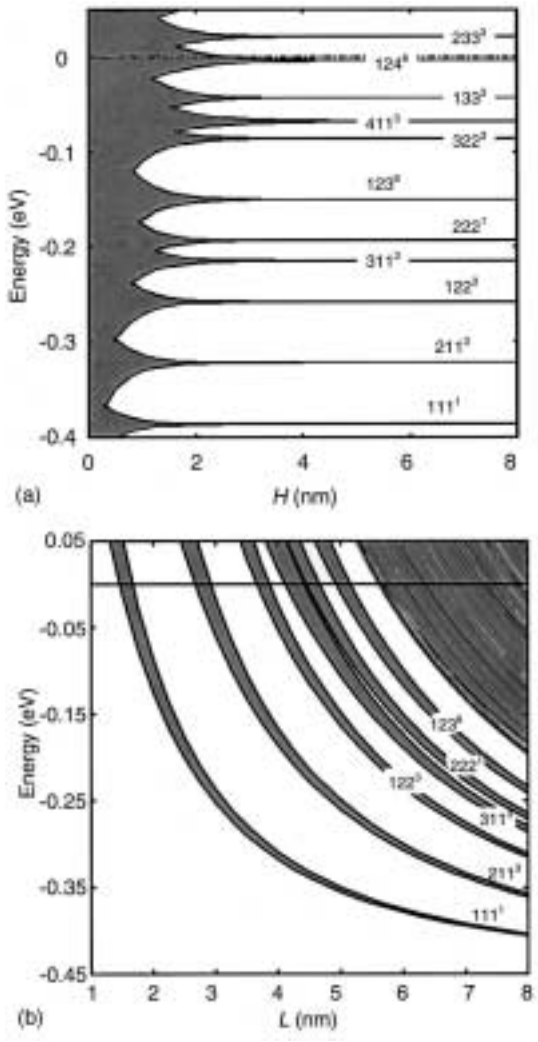

FIG. 4. (a) Miniband width as a function of the interdot distance H. The size of the dots is $L=6.5$ nm. The important observation is that even the miniband, which lies above the barrier ($E>0$), evolves to a discrete level as the interdot distance increases. (b) Miniband energy as a function of dot size. The interdot distance is $H=1.5$ nm.

crystals, the finite extend of the structure and fluctuations in the dot position will unavoidably lead to a finite linewidth of the described quasi discrete states, but the spectrum will still be different from a regular continuum.

For all suggested practical applications of single quantum dots, QDS, and QDC, it is important to know the effective mass of electrons and holes. While in single quantum dots the effective mass will be mostly defined by the material of the dot, crystallographic direction and the strain distribution, in QDC it will strongly depend on the periodicity and regimentation of the dots in the artificial crystal. A reciprocal effective mass tensor in QDC is defined as

$$\left(\frac{m_0}{M^*}\right)_{\alpha\beta}=\frac{m_0}{\hbar^2}\frac{\partial^2 E}{\partial q_\alpha \partial q_\beta}, \tag{9}$$

where α and β correspond to axes in the coordinate system associated with QDC (see Fig. 1). The simulation shows that the effective mass in QDC is highly anisotropic and strongly dependent on the miniband index, e.g., quantum numbers

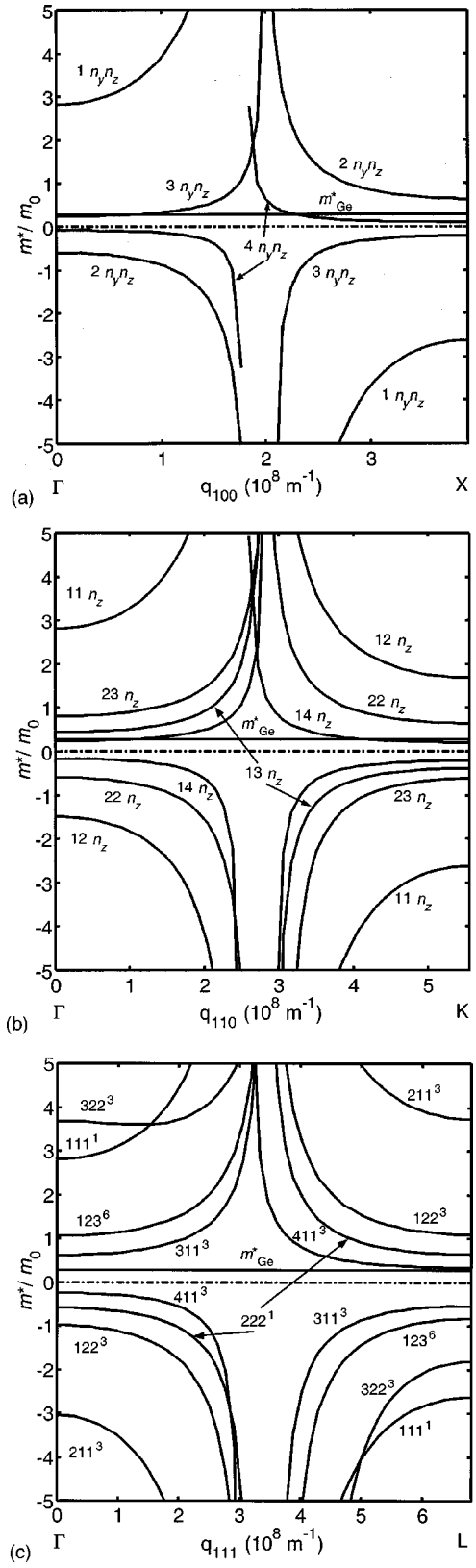

FIG. 5. Heavy-hole effective mass in a Ge/Si cubical QDC along [[100]], [[110]], and [[111]] quasi crystallographic directions. The dot size is $L = 6.5$ nm and the interdot distance is $H = 1.5$ nm.

that define the miniband [see Figs. 5(a)–5(c)]. The values of the effective mass shown in Figs. 5(a)–5(c) are normalized by the free electron mass. One can see that the effective mass in QDC is almost always different from that one in the corresponding bulk material. The effective mass in bulk Ge is also shown in the Figs. 5(a)–5(c) marked as m^*_{Ge}. The points at the Brillouin zone where the effective mass has a discontinuity of the second type are related to a bend of the corresponding dispersion branch. The branches of the negative effective mass can be easily correlated with carrier dispersion shown in Figs. 2(a)–2(c). These drastically different values of the effective mass tensor in a QDC will unavoidably lead to a modification of electronic and thermoelectric properties of semiconductor materials that comprise the artificial crystal.

The carrier motion perpendicular to the sides of quantum dots is defined by only one quantum number that describes quantization in the direction of motion. In this case a family of minibands (with the same quantum number n_x and different quantum numbers n_y and n_z) is characterized by the same effective mass [see Fig. 5(a)]. Thus, along [[100]] direction, the carrier transport in QDC is similar to the one in conventional quantum well superlattices. The effective mass along [[110]] direction is determined by two quantum numbers, so that few minibands have the same value of the effective mass [see Fig. 5(b)]. Transport along [[111]] direction, e.g., cube diagonal, is more complicated and the effective mass is different for each branch [see Fig. 5(c)]. Application of an electric field along this direction would initiate carrier transport significantly different from that in quantum well superlattices.

So far, we have limited our numerical analysis to simple cubic QDC. The formalism presented in Sec. II allows us to treat more general types of quantum dot shape and regimentation, such as tetragonal or orthorhombic QDC. As we briefly mentioned, the same symmetry of the dot and the superlattice lead to the additional degeneracy [see Figs. 2(a)–2(c)]. Once the symmetries are different, part of the degeneracy will be lifted. The latter is illustrated in Fig. 6, where we show carrier dispersion in the valence band of Ge/Si tetragonal QDC with the cubic dots ($L_x = L_y = L_z = 6.5$ nm) but with different interdot distances $H_x = H_y = 1.5$ nm, $H_z = 1.0$ nm. The dispersion is shown in [[111]] quasi crystallographic direction.[22] We have carried out calculations for a variety of other structures with different dot sizes and interdot distances. The important conclusion that was drawn from these numerical simulations is that the structure of minibands is more sensitive to the arrangement of quantum dots rather than to the shape of the dots. The latter is analogous to the observation made for real crystals, which is called the Hume–Rothery rule.[23] It states that the Brillouin zone structure depends on the basic crystal lattice, and not much on the actual ions that occupy the lattice sites.

IV. CONCLUSION

The carrier band structure in a 3D *regimented* array of semiconductor quantum dots, e.g. QDC, has been analyzed. Numerical simulations have been carried out for the valence band of a Ge/Si quantum dot crystals with parameters close to the MBE grown structures. It was shown that the coupling among quantum dots leads to a splitting of the quantized

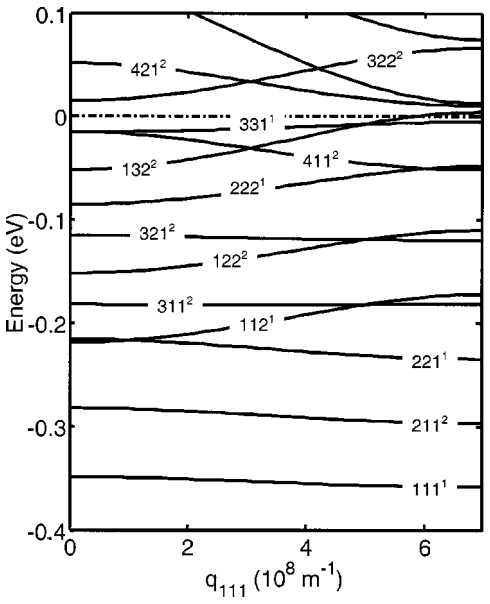

FIG. 6. Dispersion relation in a tetragonal quantum dot crystal shown along [[111]] quasi crystallographic direction. The dot sizes are $L_x=L_y=L_z=6.5$ nm. The interdot distances are $H_x=H_y=1.5$ nm and $H_z=1.0$ nm.

electron energy levels of single dots, which results in the formation of 3D minibands. By changing the size of quantum dots, interdot distances, barrier height, and regimentation, one can control the electronic band structure of this artificial crystal. It was also demonstrated that the density of electronic states and the effective mass tensor in such a crystal are significantly different from those in bulk and quantum well superlattices. The properties of the artificial crystals turned out to be more sensitive to the dot regimentation than to the dot shape.

ACKNOWLEDGMENT

The work was supported in part by the UC Energy Institute's EST program, CRDF Award MP2-2281 and the UCR Seed Grant on Nanotechnology. One of the authors (A.B.) also acknowledges UC Regents' Faculty Award. The authors thank Professors R. Lake (UCR), A. Korotkov (UCR), and K. L. Wang (UCLA) for illuminating discussions on properties of nanostructures. Numerical simulations have been performed using facilities of the Nanoelectronic Materials and Device Laboratory (NOMAD).

[1] N. N. Ledentsov, V. M. Ustinov, V. A. Shchukin, P. S. Kop'ev, Z. I. Alferov, and D. Bimberg, Semiconductors **32**, 343 (1998); O. P. Pchelyakov, Yu. B. Bolkhovityanov, A. V. Dvurechenskii, A. I. Nikiforov, A. I. Yakimov, and B. Voigtlander, Thin Solid Films **367**, 75 (2000).
[2] K. L. Wang and A. Balandin, in *Optics of Nanostructured Materials*, edited by V. Markel and T. George (Wiley, New York, 2000), p. 515.
[3] J. L. Liu, W. G. Wu, A. Balandin, G. L. Jin, and K. L. Wang, Appl. Phys. Lett. **74**, 185 (1999).
[4] J. L. Liu, W. G. Wu, A. Balandin, G. L. Jin, Y. H. Luo, S. G. Thomas, and K. L. Wang, Appl. Phys. Lett. **75**, 1745 (1999).
[5] P. C. Sharma, K. W. Alt, D. Y. Yeh, and K. L. Wang, Appl. Phys. Lett. **75**, 1273 (1999).
[6] V. Ya. Aleshkin, N. A. Bekin, N. G. Kalugin, Z. F. Krasilnik, A. V. Novikov, V. V. Postnikov, and H. Seyringer, JETP Lett. **67**, 48 (1998).
[7] G. Springholz, V. Holy, M. Pinczolits, and G. Bauer, Science **282**, 734 (1998).
[8] G. Springholz, M. Pinczolits, P. Mayer, V. Holy, G. Bauer, H. H. Kang, and L. Salamanca-Riba, Phys. Rev. Lett. **84**, 4669 (2000).
[9] A. Balandin, K. L. Wang, N. Kouklin, and S. Bandyopadhyay, Appl. Phys. Lett. **76**, 137 (2000).
[10] R. E. Ricker, A. E. Miller, D.-F. Yue, G. Banerjee, and S. Bandyopadhyay, J. Electron. Mater. **25**, 1585 (1996).
[11] K. L. Wang and P.-F. Yuh, IEEE J. Quantum Electron. **25**, 12 (1989).
[12] O. L. Lazarenkova and A. N. Pikhtin, Appl. Surf. Sci. **166**, 273 (2000); O. L. Lazarenkova and A. N. Pikhtin, Semiconductors **32**, 992 (1998).
[13] A. Khitun, A. Balandin, J. L. Liu, and K. L. Wang, J. Appl. Phys. **88**, 696 (2000).
[14] C. Goffaux, V. Lousse, and J. P. Vigneron, Phys. Rev. B **62**, 7133 (2000).
[15] M. A. Cusack, P. R. Briddon, and M. Jaros, Phys. Rev. B **54**, R2300 (1996).
[16] G. Bastard, Phys. Rev. B **25**, 7584 (1982).
[17] S. C. Jain, H. E. Maes, K. Pinardi, and I. De Wolf, J. Appl. Phys. **79**, 8145 (1996).
[18] C. G. V. de Walle and R. M. Martin, J. Vac. Sci. Technol. B **4**, 1055 (1986).
[19] M. Califano and P. Harrison, J. Appl. Phys. **88**, 5870 (2000).
[20] J. Gallaway, *Energy Band Theory* (Academic, New York, 1964).
[21] G. Bastard, *Wave Mechanics Applied to Semiconductor Heterostructures* (Halsted Press, New York, 1988).
[22] Since intersections of different branches are symmetry forbidden, they can be removed in a more accurate description by taking into account the interminiband interactions.
[23] J. M. Ziman, *Principles of the Theory of Solids* (Cambridge University Press, UK, 1964).